

Multiple-fault diagnosis in induction motors through support vector machine classification at variable operating conditions

José D. Martínez-Morales¹ · Elvia R. Palacios-Hernández² · D. U. Campos-Delgado²

Received: 10 November 2013 / Accepted: 9 November 2016 / Published online: 21 November 2016
© Springer-Verlag Berlin Heidelberg 2016

Abstract This work presents a fault diagnosis strategy for induction motors based on multi-class classification through support vector machines (SVM), and the so-called one-against-one method. The proposed approach classifies four different motor conditions (healthy, misalignment, unbalanced rotor and bearing damage) at variable operating conditions (supply frequency and load torque). The proposed SVMs use signatures from the frequency domain characteristics related to each studied fault. These signatures combine information just from the stator condition: radial vibration and stator currents. To acquire training and validation data in steady state, different experiments were performed using a three-phase induction motor. Thirty-five data sets were obtained at different operating regimes of the induction motor for each specific fault (140 conditions including a no-fault scenario) to validate our study. The SVMs with a Gaussian radial basis function (RBF) were proposed as a kernel for the nonlinear classification process. To select the parameter value of the RBF, a bootstrap technique was used. The resulting accuracy for the fault classification process was on the range 84.8–100%.

Keywords Fault diagnosis · Induction motors · Nonlinear classification

1 Introduction

Induction motors (IM) are widely used in modern industry due to their reliability, low cost and high performance; however, mechanical and electrical faults could occur in induction motors [1, 2]. Several studies have shown that almost 40–50% of all motor failures are bearing related, caused by corrosion, inadequate lubrication or installation [3]. On the other hand, a large percentage of machinery malfunctions are because of rotor unbalance and misalignment alone [2]. These faults produce excessive vibration, causing the system to eventually follow a shutdown condition, resulting in economic losses and even life-threatening conditions. Therefore, a fault condition must be detected at its early stage to avoid undesirable motor failures.

Due to the importance of fault diagnosis in IMs, a great amount of research has focused on providing reliable and robust fault detection and isolation (FDI) algorithms. According to the required information by the FDI stage, there are two main trends: motor current signature analysis (MCSA) [4–11], and vibration-based studies [12–16], where a frequency domain analysis is required for these signals to identify characteristic frequencies related to a given fault. In fact, there has been efforts looking to understand the relations between the frequency information of both signals, vibration and currents, in a fault condition [17, 18]. However, there are certain faults that have a more distinctive signature in the vibration information than in the stator current traces. In fact, recent works have focused on using the voltage and current information in electrical machines for diagnosis purposes. Hence, different types of eccentricity and short-circuit faults

This research was supported in part by the Universidad Autonoma de San Luis Potosi through an FAI grant.

✉ D. U. Campos-Delgado
ducd@fciencias.uaslp.mx

José D. Martínez-Morales
jdaniel.martinez@alumnos.uaslp.edu.mx

Elvia R. Palacios-Hernández
epalacios@fciencias.uaslp.mx

¹ Facultad de Ingeniería, Universidad Autónoma de San Luis Potosí, San Luis Potosí, Mexico

² Facultad de Ciencias, Universidad Autónoma de San Luis Potosí, San Luis Potosí, Mexico

in a synchronous machine were detected by field current and shaft voltage in [19]. Meanwhile, in [20], the active and reactive power in the electrical generator of a wind turbine are employed to detect faults in the gearbox using symmetrical components information and frequency domain data. Resistive unbalance and winding inter-turn short circuits were also studied in permanent magnet synchronous motors by zero-sequence voltage components and stator currents harmonics analysis in [21].

An important research line in IM health-monitoring has relied on artificial intelligence techniques such as artificial neural networks, fuzzy logic, genetic algorithms and support vector machines [22–36], for designing monitoring and diagnosis schemes. In [8], the application of a radial basis function (RBF) neural network is presented as a classifier to detect only bearing faults with an accuracy of 93.75%, where the inputs of the neural network are the Concordia components of the stator currents. In [12], a neural network is trained with vibration spectra obtained from an FFT-based algorithm for fault detection of half, one, two and four broken bars. On the other hand, in [17], the FFT technique was employed to convert time domain signals of the motor's vibration and stator current measurements into frequency domain information, which it is a well-recognized standard due to its simplicity and small amount of processing power, and since it can provide salient features for the diagnosis of the bearing condition under different load configurations and motor speeds. In [29], a scheme for multiple-fault diagnosis based on support vector machines (SVM) is used to detect bearing faults using electrical signals and vibrations. In [30], it is presented the application of wavelet and SVMs for detecting only bearing faults. Meanwhile, in [32], several SVM classifiers (45) are applied to perform fault diagnosis of ten conditions of rotor bars regardless of other failures in the IM. The input data are extracted from the spectral information of the motor currents, voltages and magnetic field. Recently, in [33], it has been developed a scheme using SVMs for diagnosing bearing conditions, particularly, outer race, inner race, and rolling element faults, where a 97.42% accuracy is achieved. Similarly, in [35], a fault diagnosis scheme for locomotive roller bearings have been proposed using an SVM classifier, where the parameters of the SVM are tuned by an ant colony optimization method. In addition, a learning classification method based on SVM has been successfully suggested for motor pumps of oil rigs using vibration information in [36].

Similarly, in [37], the authors propose a diagnosis scheme based on wavelet support vector machine (WSVM) and immune genetic algorithm (IGA) to determine the optimal parameters for the WSVM. With this approach, four kinds of gearbox faults are detected using vibration signals with a classification average accuracy of 97.98%. In [38], a particle swarm optimization (PSO) method is used to determine the tuning parameters of the WSVM. In this study, only

vibration signals are employed to identify different fault patterns of the rolling elements in bearings, achieving a fault classification accuracy of 96.35 and 97.5% for Mexican hat and Morlet wavelet kernels, respectively. In [39], artificial neural networks (ANNs) and SVMs are used for bearing fault detection in electrical machines, using also just time domain vibration signals. For the SVMs, the kernel parameters are selected from PSO algorithm. This approach achieved a classification success accuracy in the range 98.6–100%. In [40], the authors use the harmonics of bearing fault-related frequencies from vibration signals to detect outer race bearing faults in a three-phase squirrel-cage induction motor using SVM's. Finally, wavelet-based feature extraction of axial, radial and tangential vibration signals is employed in [41] to detect stator interturn fault and bearing damage, where SVM and k-nearest neighbor were used as classification methods.

Although there is a vast and thorough literature in FDI methods applied to IM, there are still open problems and unsolved issues, as multiple-fault diagnosis, beyond bearing failures and variable operating conditions during evaluations. This last scenario comprises variable supply frequencies and load torques. In addition by considering inverters, the robustness of the diagnosis algorithms to high-frequency switching has to be verified. Under this perspective, this paper extends and complements our early study in [29], where the novelty of this work relies on studying simultaneous fault diagnosis in IM by considering three mechanical rotor malfunctions: bearing damage, misalignment and unbalanced rotor, and assuming variable operating conditions of the system with respect to supply frequency and load torque. The unbalance rotor scenario in the IM is assumed from a mechanical origin. Other common fault conditions in IM, like eccentricity or stator shorts are outside the scope of this study, and will be the focus of future works. The studied faults produce distinctive cyclic patterns in the mechanical vibration and stator currents of the IM, as has been documented in the literature [2]. Therefore, the FFT algorithm is employed to extract frequency characteristics of the radial vibration and stator currents. Consequently, our approach combines electrical and mechanical information of the IM to construct a distinctive feature vector for multiple-fault diagnosis at variable working conditions. The multi-fault classification is achieved using SVMs with the so-called one-against-one method, which constructs classifiers where each one is trained on data from two classes. The selected SVM parameters are based on the lowest classification error obtained using bootstrapped samples in the training phase. To validate the final FDI scheme, the methodology is implemented in a LabView platform. The classification accuracy is obtained in the range of 84.8 to 100% under variable supply frequency and load torque conditions (140 operating regimes). To achieve this classification performance, this approach requires the fusion

of different information sources, as radial vibration and stator currents.

The rest of this paper is organized as follows. Section 2 presents the mathematical formulation of the SVM classifiers and the selection of their parameters. Section 3 presents the frequency components related to the studied faults in the vibration and stator currents information. The features extraction used for classification is detailed in Sect. 4 based on frequency domain data. In Sect. 5, the quantification of the proposed features is detailed, and Sect. 6 describes the implementation of the proposed multi-fault classification scheme and the experimental results. Finally, conclusions are given in Sect. 7.

2 Support vector machine

SVM is a type of learning algorithm introduced by Vapnik and co-workers [42]. In a classification process, the SVM separates a set of binary-labeled training data with a hyperplane that maximizes its distance to the data, this is called *maximal margin hyperplane*, so the SVM can work in combination with *kernel functions*, to compute a nonlinear mapping to the features space. The hyperplane obtained by the SVM in the features space corresponds to a nonlinear decision boundary in the input space.

In a two-class classification problem with linearly separable data and l training samples, the design algorithm for an SVM is reduced to the next primal convex optimization problem

$$\begin{aligned} \min_{\mathbf{w}} \quad & \frac{1}{2} \|\mathbf{w}\|^2, \\ \text{s.t.} \quad & y_i(\mathbf{w}^\top \mathbf{x}_i + b) \geq 1, \quad \forall i = 1, \dots, l \end{aligned} \tag{1}$$

where $\mathbf{x}_i \in \mathbb{R}^n$ is the i th features sample, $y_i \in \{-1, +1\}$ is the class label value (binary problem), $\mathbf{w} \in \mathbb{R}^m$ is a weight vector, b is a bias term, and $\mathbf{w}^\top \mathbf{x}_i + b = 0$ is the decision function (hyperplane). The previous optimization problem can be represented by the next dual problem as

$$\begin{aligned} \max_{\alpha_i} \quad & \sum_{i=1}^l \alpha_i - \frac{1}{2} \sum_{i=1}^l \sum_{j=1}^l \alpha_i \alpha_j y_i y_j \langle \mathbf{x}_i, \mathbf{x}_j \rangle, \\ \text{s.t.} \quad & \sum_{i=1}^l \alpha_i y_i = 0, \quad 0 \leq \alpha_i \quad \forall i = 1, \dots, l \end{aligned} \tag{2}$$

where α_i are the Lagrange multipliers, and $\langle \mathbf{x}_i, \mathbf{x}_j \rangle$ is the inner product of the input features vectors \mathbf{x}_i and \mathbf{x}_j . The dual optimization problem can be solved numerically using MATLAB or SCILAB (commands `quadprog` and `quapro`, respectively). Next, the weight vector \mathbf{w} can be computed by

$$\mathbf{w} = \sum_{i=1}^l \alpha_i y_i \mathbf{x}_i \tag{3}$$

which is a linear combination of the input features vectors $(\mathbf{x}_1, \dots, \mathbf{x}_l)$. Then, considering the primal optimization problem in (1), the bias term b is obtained as

$$b = \max_{\substack{1 \leq i \leq l \\ \text{s.t. } y_i = -1}} \mathbf{w}^\top \mathbf{x}_i + \min_{\substack{1 \leq i \leq l \\ \text{s.t. } y_i = 1}} \mathbf{w}^\top \mathbf{x}_i. \tag{4}$$

In (2), the only term that depends on the features vectors is the inner product $\langle \mathbf{x}_i, \mathbf{x}_j \rangle$. Hence, for a nonlinear classification, the inner product is defined in a higher dimensional space through the nonlinear mapping $\phi : \mathbb{R}^n \mapsto \mathbb{R}^m$ with $m > n$. Therefore, this term can be expressed as a kernel function in the optimization procedure by

$$K(\mathbf{x}_i, \mathbf{x}_j) \triangleq \langle \phi(\mathbf{x}_i), \phi(\mathbf{x}_j) \rangle. \tag{5}$$

For the design of the SVMs, the Gaussian RBF kernel is considered:

$$K(\mathbf{x}_i, \mathbf{x}_j) = \exp\left(-\frac{\|\mathbf{x}_i - \mathbf{x}_j\|^2}{2\sigma^2}\right), \tag{6}$$

where $\|\cdot\|$ denotes the Euclidean norm, and σ is a free parameter related to the dispersion of the support vectors. In fact, the selection of the type of kernel function depends on the classification problem. Nonetheless, RBF functions have been documented extensively in the literature, making them a benchmark for classification applications based on SVMs. Summarizing, the synthesis of the SVM can be described in two steps:

- Solve the dual optimization problem (2) replacing $\langle \mathbf{x}_i, \mathbf{x}_j \rangle$ with the proposed kernel $K(\mathbf{x}_i, \mathbf{x}_j)$ in (6) to compute the terms α_i .
- Obtain \mathbf{w} and b from (3)–(4).
- Compute the optimal separation hyperplane by $\mathbf{w}^\top \mathbf{x} + b = \sum_{i=1}^l \alpha_i y_i K(\mathbf{x}_i, \mathbf{x}) + b$.

2.1 Multi-classification problem

To separate more than two fault classes in an IM, a multi-classification method is necessary. In this study, the one-against-one method is adopted, in which SVMs are constructed for all possible pairs of classes, that is, $N(N - 1)/2$ decision functions, where N is the number of classes. Since there are 4 classes (healthy, misalignment, unbalance and bearing damage), 6 SVMs are employed to separate the following class pairs: (i) healthy-misalignment (SVM1), (ii) healthy-unbalance (SVM2), (iii) healthy-bearing damage (SVM3), (iv) misalignment-unbalance (SVM4), (v)

misalignment-bearing damage (SVM5), and (vi) unbalance-bearing damage (SVM6). For this purpose, the decision function that separates the i th from the j th class for the features vector $\mathbf{x} \in \mathbb{R}^n$ is defined as

$$d_{ij}(\mathbf{x}) \triangleq \mathbf{w}_{ij}^T \mathbf{x} + b_{ij}, \quad \forall i, j = 1, \dots, N,$$

where $\mathbf{w}_{ij} \in \mathbb{R}^n$ is a weight vector and $b_{ij} \in \mathbb{R}$ a bias term. If a new pattern \mathbf{x} belongs to the set

$$\Omega_i = \{\mathbf{z} \in \mathbb{R}^n \mid \text{sign}(d_{ij}(\mathbf{z})) = +1, \forall j = 1, \dots, N; j \neq i\},$$

where $\text{sign}(\cdot)$ denotes the sign function, then \mathbf{x} belongs to class i . If \mathbf{x} does not belong to any set Ω_i for $i = 1, \dots, N$, the classification cannot be achieved by a voting scheme. For this purpose, the number of times that the features vector \mathbf{x} is assigned to the i th class is computed by

$$d_i(\mathbf{x}) = \sum_{\substack{j=1, \\ j \neq i}}^N \text{sign}(d_{ij}(\mathbf{x})). \quad (7)$$

Then, the following decision function is considered

$$d(\mathbf{x}) = \arg \max_{i=1, \dots, N} d_i(\mathbf{x}). \quad (8)$$

That is, if $d(\mathbf{x})$ is maximum for a given value of i , then \mathbf{x} belongs to i th class. The highest number of votes that a features vector \mathbf{x} may have is $N - 1$, then if $\mathbf{x} \in \Omega_i$, $d_i(\mathbf{x}) = N - 1$ and $d_k(\mathbf{x}) < N - 1$ for $k \neq i$.

2.2 SVM parameter selection

To select the parameter σ of the RBF kernel function in (6), a bootstrap technique, introduced by [43] is used for assessing accuracy of the SVM classifiers. Let $\mathbf{Z} = (\mathbf{z}_1, \mathbf{z}_2, \dots, \mathbf{z}_M)$ the training data set with M samples, where $\mathbf{z}_i = (\mathbf{x}_i, y_i)$ is a pair of features vector and class label. Next, subsets $\mathbf{Z}^b \subset \mathbf{Z}$ are randomly extracted from the training set \mathbf{Z} , this procedure is done B times, i.e., $b = 1, \dots, B$. Then, the classification error is calculated for each one of the bootstrapped samples and the behavior of the B replications is examined. If $d(\mathbf{x}_i)$ is the classification result from the SVM fitted to the b th bootstrapped sample, the estimation of the SVM classification error can be given by

$$E_{\text{boot}} = \frac{1}{B \cdot M} \sum_{b=1}^B \sum_{(\mathbf{x}_i, y_i) \in \mathbf{Z}^b} (y_i - d(\mathbf{x}_i))^2. \quad (9)$$

This parameter characterizes the SVMs accuracy and can be used to choose the best classifiers.

3 Fault conditions

In this work, the classification process will be carried out based on the steady-state frequency domain characteristics of the stator currents and radial vibration measurements after a fault is present in the IM [2]. Thus, in this section, the characteristic fault frequency components for both measurements will be reviewed. Three common rotor fault conditions in induction motors will be studied: misalignment, unbalanced rotor, and bearings degradation. In the literature, there is evidence that the correct diagnosis of these three fault conditions is a challenging task, especially for variable frequency and load torque conditions [3]. One important remark is that the resulting frequency components produced by the studied faults are dependent on the supply frequency of the IM, but independent of its power rating [2,3], as will be described next.

3.1 Misalignment fault

Misalignment is produced by an inaccurate coupling between the IM shaft and its load. This condition can induce oscillations in the air-gap length that cause variations in the air-gap flux density. In fact, misalignment affects the equivalent inductances of the machine producing stator current harmonics at the following frequencies [2]:

$$\begin{aligned} f_m &= f_s \left[1 \pm k \left(\frac{1-s}{p} \right) \right], \\ &= f_s \pm k f_r, \quad k = 1, 2, \dots \end{aligned} \quad (10)$$

where f_s denotes the electrical supply frequency, s is the slip, p the number of pole pairs and f_r the mechanical rotor speed. At the same time, misalignment produces components in the spectrum of the radial vibration signal at frequencies f_r and $2f_r$. However, the dominant component is located at $2f_r$. In addition, when the misalignment is severe, it is possible to find other harmonics from $3f_r$ to $8f_r$, or even a whole series of high-frequency harmonics [3].

3.2 Unbalance rotor fault

Unbalance is characterized by an uneven distribution of mass about the IM rotating centerline (mechanical origin) [3]. The addition of keys and keyways helps to avoid the unbalance condition in IM, where the ISO 8821 standard establishes conventions for shaft and fitment key, but in practice, different manufacturers follow their own procedures as to use a full key or half key. The source of these failures can be the imprecision in manufactured parts that produce concentricity and unbalance individually. Thus, when a motor is assembled and the permanent key is added, unbalance will often be the result. Moreover, looseness of parts can result in shifting dur-

ing operation, causing a change in balance, other factors as corrosion, wear and deposit build up that can lead to severe unbalance, particularly to fans, blowers and compressors.

Due to the small amplitude of the fault harmonics in current spectrum, when this fault is emerging is difficult to be detected; therefore, we used the vibration information. However, the faults considered in this paper are detected when they are already present and not in the emerging phase. Similarly to a misalignment fault, an unbalanced rotor causes variations in the air-gap length, so it is expected components once more at fault frequencies $f_m = f_s \pm kf_r$ $k = 1, 2, \dots$ in the spectrum of the stator currents [2]. Although there are similarities in the electrical diagnostic media for misalignment and unbalanced rotor, the frequency information of the vibration signal provides additional insight. For a case of unbalance, there is a predominant component of vibration signal at the rotational speed of the machine f_r in the radial direction [3].

3.3 Bearing faults

The frequency spectrum of the vibration signal related to a bearing failure can be split into four zones, observed as the bearing wear progresses [3], these zones are at (i) rotational speed machine and harmonics, (ii) bearing defect frequencies zone (80–500 Hz), (iii) bearing component natural frequencies zone (500–2 kHz), and (iv) high-frequency zone (beyond to 2 kHz). As a result, features in the frequency spectrum of the vibration signal can be isolated according to the severity of the wear. For example, for an IM with an incipient bearing defect, the frequency components present in the vibration information refer to zone in the 500 Hz to 2 kHz range. At this stage, the fatigued raceways begin to develop minute pits, where as the rolling elements pass over these pits, the ringing or the bearing component natural frequencies are generated [3]. There are several studies of bearing fault diagnosis using stator currents information [14], as the Hilbert modulus current space vector (HMCSV) and Hilbert phase current space vector (HPCSV) [44]. However, this study shows that the vibration measurements provide key information for multi-class fault detection [39].

4 Features extraction

The first step in the design of an FDI scheme is to define residual signals of the process, i.e., signals that will change their time or frequency patterns when a fault appears. From the analysis in the previous section, stator currents and radial vibration can serve for this purpose. In fact, only the measurement of one stator current could be enough due to the symmetry in the IM. Nevertheless, due to pulse-width-modulation (PWM) inverters and electrical noise, the

frequency components in the stator current could be affected. In addition, all IMs have an intrinsic stator unbalance due to the manufacturing process. So, we include a residual based on Clarke transformation of the three stator currents [7]. As will be shown in the next section, this extra information allows separability in the features space. The mathematical foundation of this residual is detailed next.

In the presence of a misalignment fault, the stator currents spectrum will contain components at frequencies described in (10). These new components could be viewed as sideband elements of the supply frequency f_s . Clarke transformation is used to obtain a two-dimensional representation of the three-phase IM stator currents, [4,5,7]. As a function of the stator currents (i_a, i_b, i_c) , Clarke vector is represented by $\mathbf{i}_{dq} = [i_d \ i_q]^T$ whose components are:

$$\begin{cases} i_d = \sqrt{\frac{2}{3}}i_a - \frac{1}{\sqrt{6}}i_b - \frac{1}{\sqrt{6}}i_c, \\ i_q = \frac{1}{\sqrt{2}}i_b - \frac{1}{\sqrt{2}}i_c. \end{cases} \quad (12)$$

Hence, the squared magnitude of Clarke vector is

$$\|\mathbf{i}_{dq}\|^2 = i_d^2 + i_q^2. \quad (13)$$

Evaluating (13), the spectrum of Clarke vector modulus will have components at frequencies $2f_s, 2f_s \pm f_r, 2f_s \pm 2f_r, f_r$ and $2f_r$, in addition to a DC level [4,5]. Consequently, there are two distinctive components at the rotational frequency f_r and its second harmonic $2f_r$ related to the misalignment fault in this residual.

5 Features quantification

The fault diagnosis scheme relies on a features vector to achieve accurately the multi-classification process of the IM condition, and next, the features vector is classified using a voting scheme based on SVMs. The features proposed in this work are the amplitudes of the spectral components at the distinctive fault frequencies for each diagnostic element. An FFT is then performed to extract the frequency characteristics of the stator current, Clarke vector modulus and vibration measurement. The power spectral density (PSD) for each signal is

$$P_k^c = |D^c(k)|^2, \quad (14)$$

where $D^c(k)$ is the Discrete Fourier Transform of signal $c(n)$

$$D^c(k) = \sum_{n=0}^{N-1} c(n)e^{-j2\pi kn/N} \quad k = 0, 1, \dots, N-1,$$

N is the number of samples of $c(n)$, $0 \leq n \leq N - 1$. In this study, the stator current of phase- a in the IM (i_a), Clarke vector modulus ($\|i_{dq}\|$), and the vibration signal (v) are sampled at a frequency of $f = 40$ kHz with a time window of 800,000 samples, i.e., an acquisition time window of 20 s. Then the resolution in the PSD is $\Delta f = f/N = 0.05$ Hz. From the experimental measurements, the minimum resolution necessary to obtain accurate classification results is 0.05 Hz. The data acquisition card is equipped with a low-pass filter (cutoff frequency of 40 kHz), which is used to eliminate electrical noise in the signals. Note that the frequency resolution is important, because in a noisy spectrum a fault-related spectral component could be overlooked. From the information of a stator current (i_a), Clarke vector modulus ($\|i_{dq}\|$), and mechanical vibration (v) are extracted six distinctive features:

- (i) ζ_{i_a} → energy of the frequency components in the line current at frequencies $f_s + f_r, f_s + 2f_r, f_s + 3f_r, f_s + 4f_r$.
- (ii) $\zeta_{\|i_{dq}\|}$ → energy of the frequency components in Clarke vector modulus at frequencies $f_r, 2f_r$ and $4f_r$.
- (iii) ζ_v^1 → energy of the component at frequency f_r in the radial vibration measurement.
- (iv) ζ_v^2 → energy of the components at frequencies $2f_r$ and $3f_r$ in the radial vibration measurement.
- (v) ζ_v^3 → energy of the components at frequencies $5f_r, 6f_r$ until 900 Hz in the radial vibration measurement.
- (vi) ζ_v^4 → energy of the components in the range 1500 to 1800 Hz in the radial vibration measurement.

Therefore, according to the description of the fault components in Sect. 3, ζ_{i_a} and $\zeta_{\|i_{dq}\|}$ are characteristics obtained from the stator current and Clarke vector modulus, related to misalignment and unbalance faults. ζ_v^2 and ζ_v^3 are characteristics obtained from the vibration signal related to a misalignment fault. Finally, ζ_v^1 and ζ_v^4 are characteristics obtained from the vibration signal associated with unbalance and bearing faults, respectively. Next, the mathematical descriptions of these indexes based on (14) and measurements ($i_a, \|i_{dq}\|, v$) are presented:

$$\zeta_{i_a} = \sum_{k=k_s+k_r-10}^{k_s+k_r+10} P_k^{i_a} + \sum_{k=k_s+2k_r-10}^{k_s+2k_r+10} P_k^{i_a} + \sum_{k=k_s+3k_r-10}^{k_s+3k_r+10} P_k^{i_a} + \sum_{k=k_s+4k_r-10}^{k_s+4k_r+10} P_k^{i_a}, \tag{15}$$

$$\zeta_{\|i_{dq}\|} = \sum_{k=k_r-10}^{k_r+10} P_k^{\|i_{dq}\|} + \sum_{k=2k_r-10}^{2k_r+10} P_k^{\|i_{dq}\|} + \sum_{k=4k_r-10}^{4k_r+10} P_k^{\|i_{dq}\|}, \tag{16}$$

$$\zeta_v^1 = \sum_{k=k_r-10}^{k_r+10} P_k^v, \tag{17}$$

$$\zeta_v^2 = \sum_{k=2k_r-10}^{2k_r+10} P_k^v + \sum_{k=3k_r-10}^{3k_r+10} P_k^v, \tag{18}$$

$$\zeta_v^3 = \sum_{k=5k_r-10}^{5k_r+10} P_k^v + \sum_{k=6k_r-10}^{6k_r+10} P_k^v + \dots + \sum_{k=\lfloor 18000/k_r \rfloor k_r - 10}^{\lfloor 18000/k_r \rfloor k_r + 10} P_k^v, \tag{19}$$

$$\zeta_v^4 = \sum_{k=30000}^{36000} P_k^v, \tag{20}$$

where $\lfloor \cdot \rfloor$ denotes the floor function, index $k_s = f_s/\Delta f$ represents the sample number corresponding to the supply frequency f_s , and $k_r = f_r/\Delta f$ with respect to the rotational speed of the IM. The estimated energy of the harmonic components at rotational frequency f_r is carried out over a window of ± 0.5 Hz for indexes in (15)–(19). Therefore, the features vector \mathbf{x} given over a time window is denoted by

$$\mathbf{x} = [\zeta_{i_a}, \zeta_{\|i_{dq}\|}, \zeta_v^1, \zeta_v^2, \zeta_v^3, \zeta_v^4]^T \in \mathbb{R}^6. \tag{21}$$

where each component of the features vector \mathbf{x} contains the power carried by the respective signal, per unit frequency, known as the PSD of the signals. The PSD of these signals is expressed in watts per hertz (W/Hz). The indexes in equations (15)–(20) are established according to correspondence between the fault frequencies and the range of samples in the PSD. The relationships between the frequency range of the faults and the number of samples in the spectrum of each diagnostic media are shown in Table 1.

Figure 1 shows the general scheme of the proposed fault diagnosis strategy based on SVMs. In this scheme, the measurements are given by stator currents, radial vibration, supply frequency and shaft speed of the machine. Next, after data acquisition, the diagnosis architecture is programmed in LabView to compute in real time the health assessment of the IM. Hence, the program performs Clarke transformation over the current measurements, and the FFT of the radial vibration, stator current and Clarke vector modulus signals to compute the features vector \mathbf{x} .

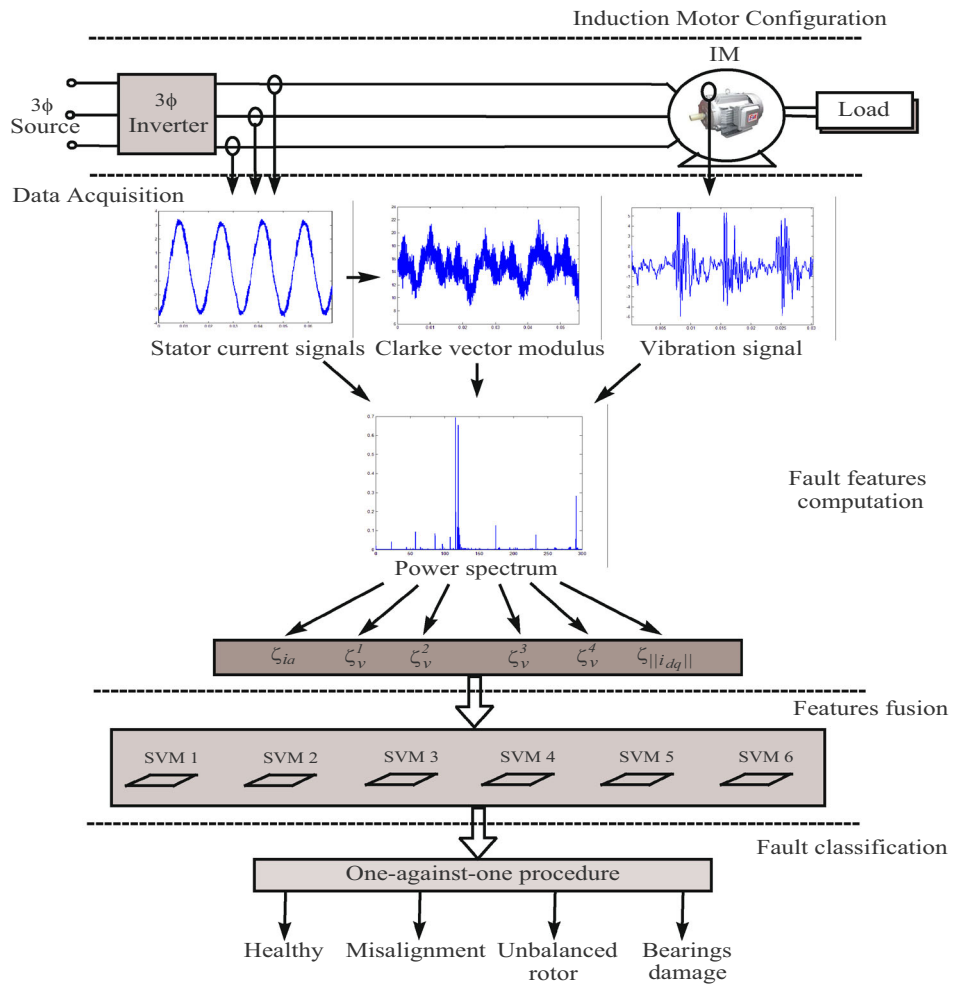
6 Experimental results

To observe and analyze the frequency information produced by the studied faults, the kit “Machine Fault Simulator” from SpectraQuest, Inc., shown in Fig. 2 is employed. The IM is supplied from a three-phase power inverter Altivar 11

Table 1 Relationship between the frequency range of the faults and the number of sample in the spectrum of each diagnostic media

| No. of sample | $k_s + k_r \pm 10$ | $k_r \pm 10$ | $k = 30,000$ | $k = 36,000$ |
|---------------|------------------------|------------------|--------------|--------------|
| Frequency | $f_s + f_r \pm 0.5$ Hz | $f_r \pm 0.5$ Hz | 1500 Hz | 1800 Hz |

Fig. 1 SVM motor fault detection system



of 1.5 kW. The motor shaft is coupled to a gearbox by a belt drive system used to load the motor with a permanent magnet brake (Precision Tork). The brake can be adjusted to provide a constant torque of 87.56 to 1751.26 Nm. The IM used in the test bench has the following specifications: 60 Hz, 375 W, two-pole ($p = 2$), 230/469 V, and 2.2/1.1 A. The test bench consists of four IMs with a predefined status: healthy, rotor misalignment, unbalanced rotor and bearing damage. Although the IM used is of $p = 2$ and 375 W, this machine is useful to show the applicability of the proposed methodology to solve the multi-fault classification problem, since it presents the same frequency components in the radial vibration and stator currents described in Sect. 3 by the studied faults. Moreover, these machines are still being used for low-power applications and research, as in [45], which uses

SVMs applied to an induction motor of $p = 2$ for rolling element bearing fault detection.

Figure 3a illustrates the unbalance rotor, for this purpose, screws are attached to disks mounted over the motor shaft, such that when the shaft rotates unequal centrifugal forces are generated inducing the fault. For the misalignment fault, metal shims are stacked under a machine foot, generating a shaft misalignment, as is shown in Fig. 3b. Meanwhile, for the bearing fault, the IM provided by SpectraQuest contains fixed bearings on both sides with wearing on the inner and outer raceways. Therefore, at this stage, our classification scheme cannot distinguish between a failure in inner or outer raceways, but only as a general bearing fault. Each bearing contains 9 balls, with a ball diameter of 7.94 mm, outer race diameter of 31.38 mm, and inner race diameter of 47.26 mm.

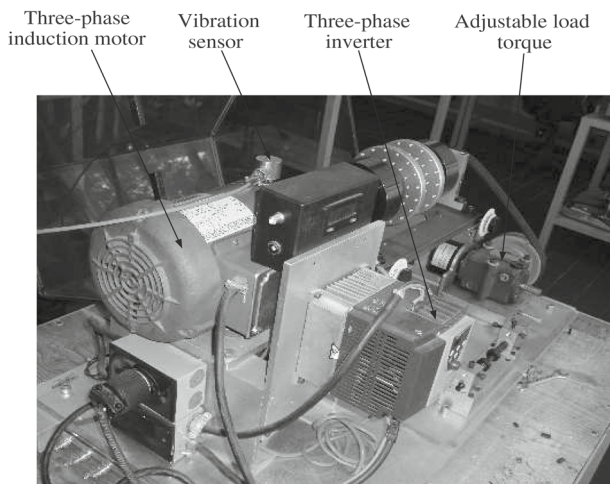


Fig. 2 Experimental setup of “Machine Fault Simulator”

The fault severity of unbalance rotor and misalignment could be increased or modified, for the unbalance rotor, by increasing the distribution of screws mounted over the disks, and for the misalignment fault, by increasing the metal shims. However, this work is focused just on the ability of detecting multiple faults, and in a future work, the fault identification or quantification will be addressed.

Each faulty motor reproduces the frequency components in the current and vibration measurements reported in the literature [2]. To obtain measurements of the stator currents, Clarke vector modulus and radial mechanical vibration, a data acquisition card NI-DAQ-9172 is used. The board is installed in a Pentium Dual Core, 2.5 GHz PC. For the vibration measurements, an accelerometer from ICP® (model 604B31) is used with a measurement range of $\pm 490 \text{ m/s}^{-2}$ and a frequency bandwidth of 0.5 Hz to 5 kHz, which is suitable for acquiring acceleration signals generated by the vibration of the studied mechanical faults.

On the other hand, the mechanical speed of the IM has to be measured, to normalize the frequency components in

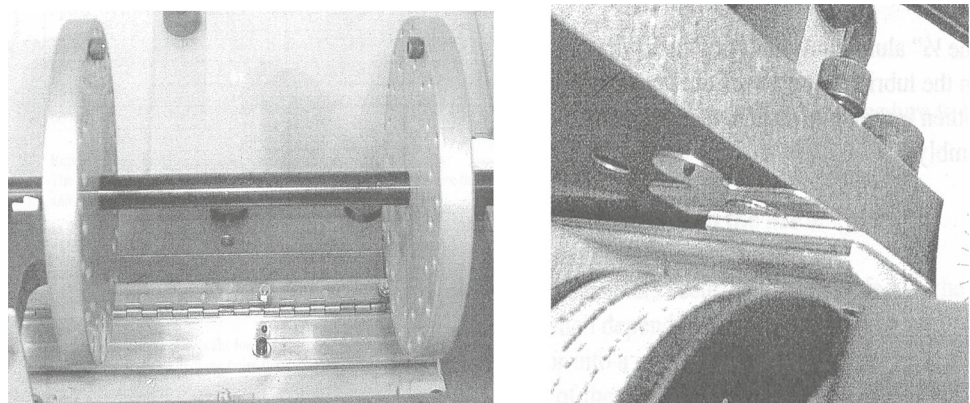
the stator current, Clarke vector modulus and radial vibration measurement. For this purpose, an infrared sensor is employed to measure the rotational frequency, which consists of an infrared light emission diode (LED) and a photodiode. This sensor provides a +5 V pulse after each complete rotation of the shaft. Next, this signal is processed by the LabView software to extract an estimation of the rotational frequency. The resolution of the measurements is 40,000 samples/s, provided by data acquisition card NI-DAQ-9172. As a result, the overall diagnosis algorithm requires information from stator currents, radial vibration and mechanical speed to achieve multiple-fault diagnosis at variable operating conditions in the supply frequency and load torque; where these last two measurements (vibration and mechanical speed) allow to expand the diagnosis capability from standard MCSA.

Figure 4 compares the frequency information of one stator current and Clarke vector modulus of the healthy response with respect to two studied fault conditions: misalignment and unbalance (supply frequency $f_s = 60 \text{ Hz}$ and maximum load torque). Hence, the frequency components predicted for ζ_{i_a} and $\zeta_{\|i_{dq}\|}$ by the analysis in Sect. 5 are present in Fig. 4. We point out that due to the induced faults, the rotational frequency is different for the misalignment ($f_r = 57.65 \text{ Hz}$) and unbalance rotor ($f_r = 58.25 \text{ Hz}$) scenarios despite that the supply frequency f_s and load torque do not change. Now, Fig. 5 shows the radial vibration for the three studied faults: bearing damage, unbalance rotor, and misalignment (supply frequency $f_s = 60 \text{ Hz}$ and maximum load torque). Similar to Fig. 4, the frequency terms captured by $(\zeta_v^1, \zeta_v^2, \zeta_v^3, \zeta_v^4)$ in the radial vibration and described in Sect. 5 are visualized in Fig. 5.

6.1 Features map

For illustration purposes, Fig. 6 shows the resulting current features, stator current feature ζ_{i_a} and Clarke vector feature $\zeta_{\|i_{dq}\|}$, versus vibration feature ζ_v^4 , as can be observed from

Fig. 3 Fault emulation of **a** unbalance rotor and **b** misalignment



(a)

(b)

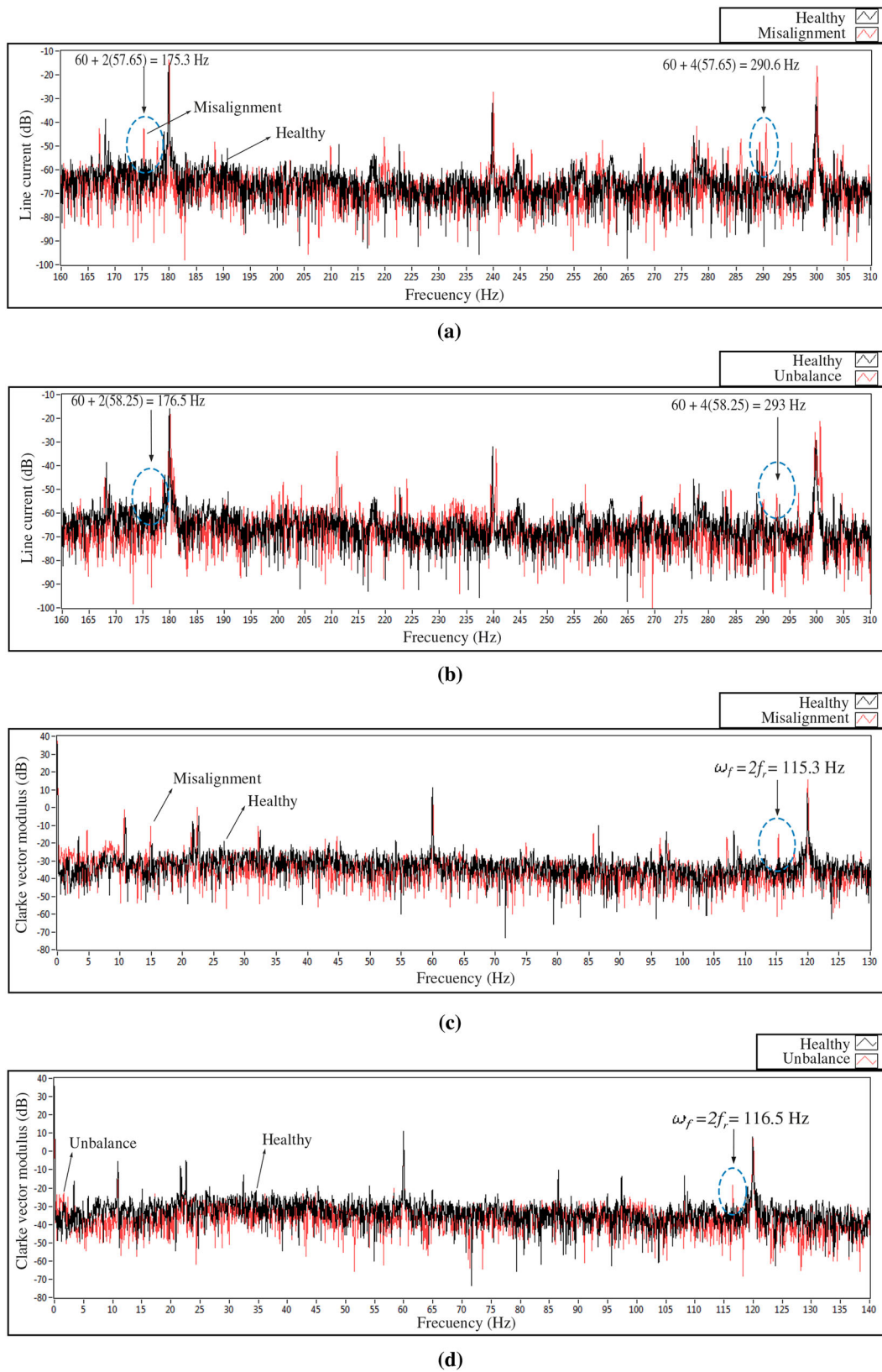


Fig. 4 Electrical diagnostic information in frequency domain (supply frequency of 60 Hz and maximum load torque): **a** stator current for healthy and misalignment conditions, **b** stator current for healthy

and unbalance rotor scenarios, **c** Clarke vector modulus for healthy and misalignment conditions, **d** Clarke vector modulus for healthy and unbalance rotor scenarios

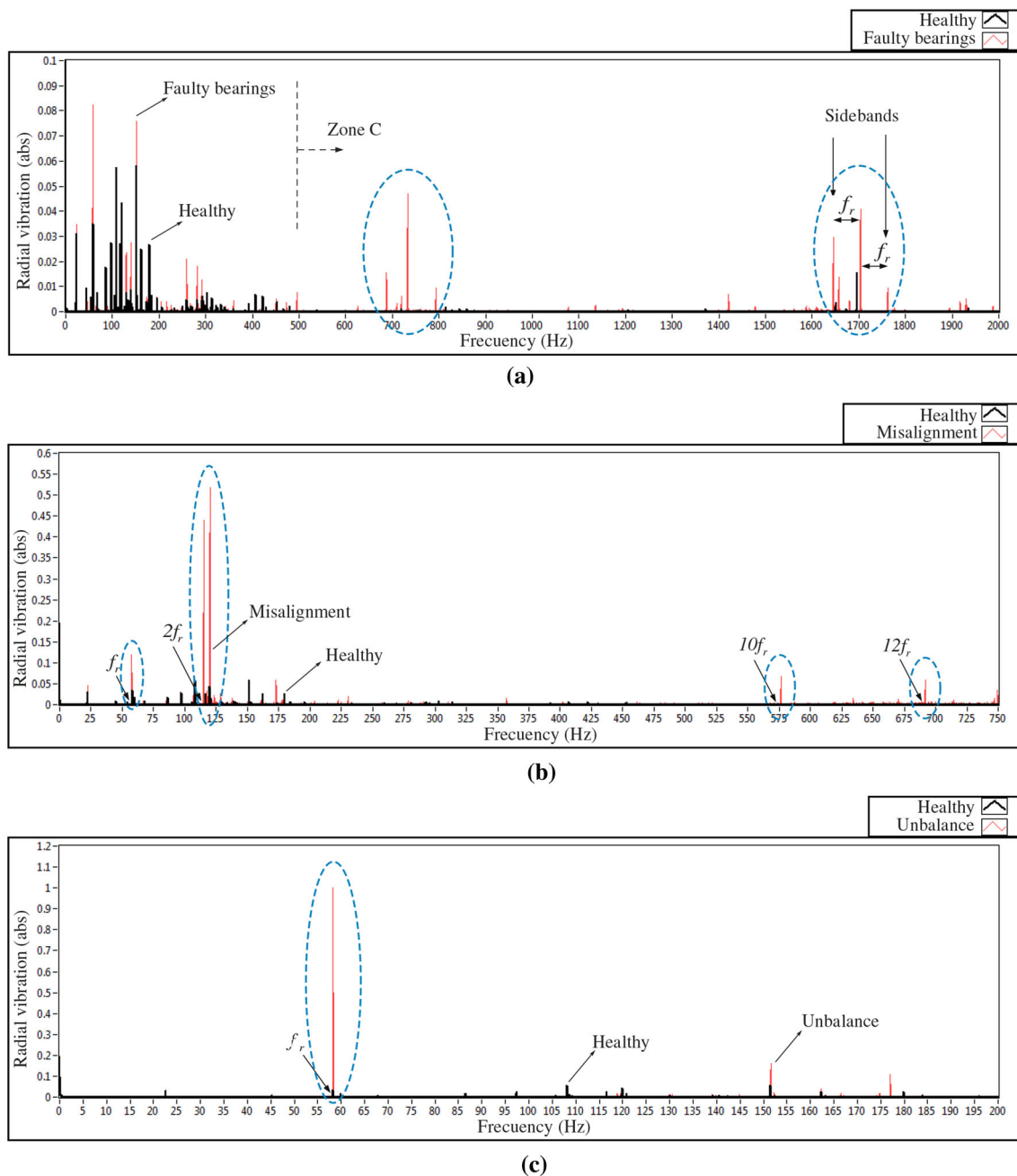


Fig. 5 Radial vibration in frequency domain (supply frequency of 60 Hz and maximum load torque): **a** bearings damage, **b** misalignment scenario, and **c** unbalance rotor fault

the plot some training points for the unbalanced rotor and misalignment faults lie in the same region of the features space. However, using information from mechanical vibration of the IM, the data of the studied faults become separable, this is shown in the plot for the vibration features ζ_v^1 , ζ_v^2 and ζ_v^3 in Fig. 7. Although the vibration sensor represents an extra cost in the fault diagnosis scheme, the economic losses caused by a fault in the induction motors of a production line could be larger.

In Figs. 6 and 7 are shown all data used for training and testing phases, that is, 35 data sets for each one of the 4 IM conditions (healthy, misalignment, unbalance, and bearing fault), for different load levels in the range of 350.25 to 1751.26 Nm and supply frequencies of 30, 40, 50 and 60 Hz. In addition, note that measurement noise will have a minimal effect on the resulting classification accuracy, since the main noise component in the stator current and vibration signals is coming from high-frequency switching of the variable

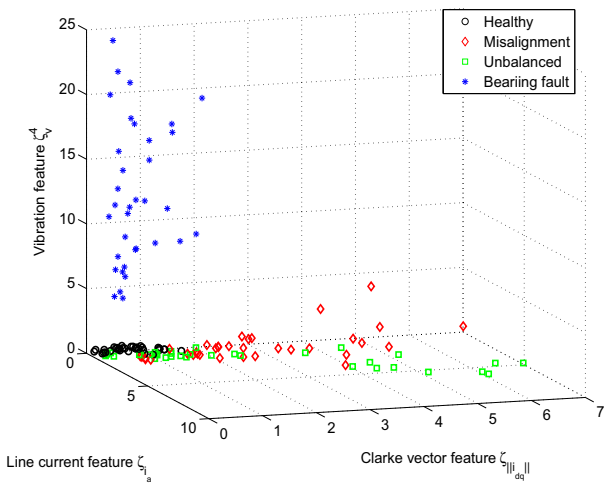


Fig. 6 Features map ζ_v^4 vs. ζ_{i_a} vs. $\zeta_{\|i_{dq}\|}$

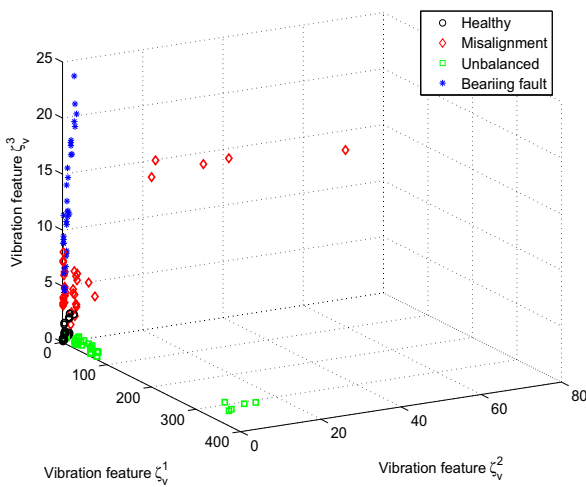


Fig. 7 Features map ζ_v^1 vs. ζ_v^2 vs. ζ_v^3

speed drive of the IM (usually >2500 Hz). However, since the classification features are located in the low-frequency side (<1800 Hz according to Table 1), the noise effect in the resulting FDI is negligible.

Although there is no overlap in the failure frequency ranges, the features for each fault are also based on the magnitude of the frequency components at specific ranges for the mechanical and electrical signals. In fact, for a healthy IM due to non-ideal manufacturing and noise, the frequency components at the fault ranges could not be zero, and this scenario makes the classification process a non-trivial task. As can be seen in Figs. 6 and 7, the data sets for each fault are not linearly separable. Therefore, nonlinear classifiers as SVMs have to be employed to solve the multi-classification problem.

6.2 SVM training

To collect the training and testing data sets, IMs with faulty and healthy conditions were run at different speeds and load

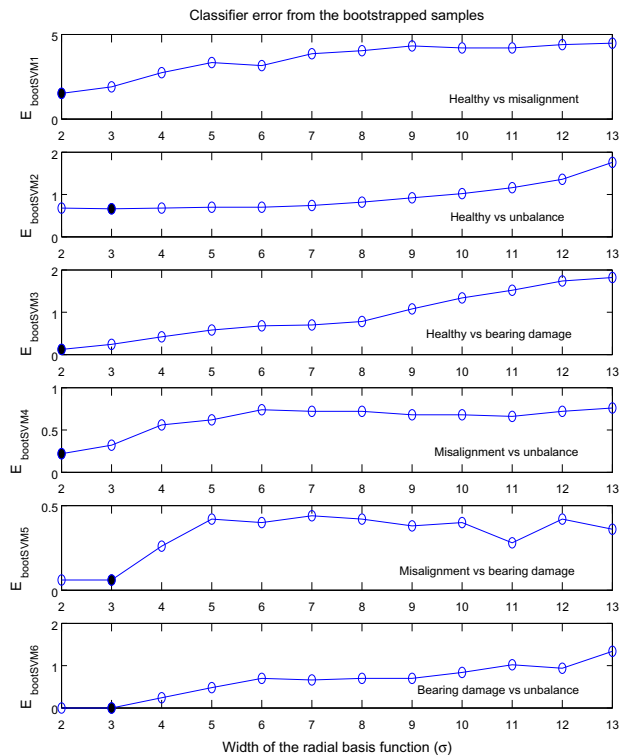


Fig. 8 Error in bootstrapped samples for the training phase

torques, and the features vector were extracted. The load levels were in the range of 350.25–1751.26 Nm, and the supply frequencies are 30, 40, 50 and 60 Hz. In total, 35 data sets were acquired for the design and evaluation of the multi-classification scheme. The training data for the 6 SVMs detailed in Sect. 2.1 included 10 sets, which were chosen randomly $B = 10$ times and according to the bootstrapped technique (see Sect. 2.2), where the validation data gathered 25 samples for each IM condition. For the training stage, the parameters of the Gaussian RBF (σ 's) in (6) were selected to minimize the error in (9), see Fig. 8. Note that the values for σ of (2, 3, 2, 2, 3, 3) provided less error in training each SVM for the bi-classification problem.

For illustration purposes, Fig. 9a presents the binary classification of data from an IM without fault (healthy) and one with misalignment, through features ζ_v^3 and $\zeta_{\|i_{dq}\|}$. Thus, by applying the sign function to the decision surface $d(\mathbf{x}, \alpha^*)$, the correct classification of the fault ($y = -1$) is obtained, as is shown in Fig. 9b. Another example is described in Fig. 10a, where the classification is shown between a misaligned IM and another with mechanical unbalance, through only the electrical diagnostic media ζ_{i_a} and $\zeta_{\|i_{dq}\|}$. Hence, even though the data are not linearly separable, the SVM can effectively achieve the nonlinear classification with a good degree of precision. Note that the intersection of the decision function $d(\mathbf{x}, \alpha^*)$ with the plane of features defines the optimal separation hyperplane, as shown in Fig. 10b.

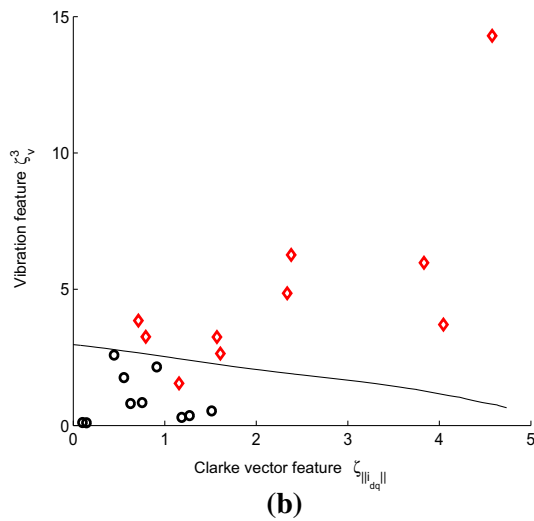
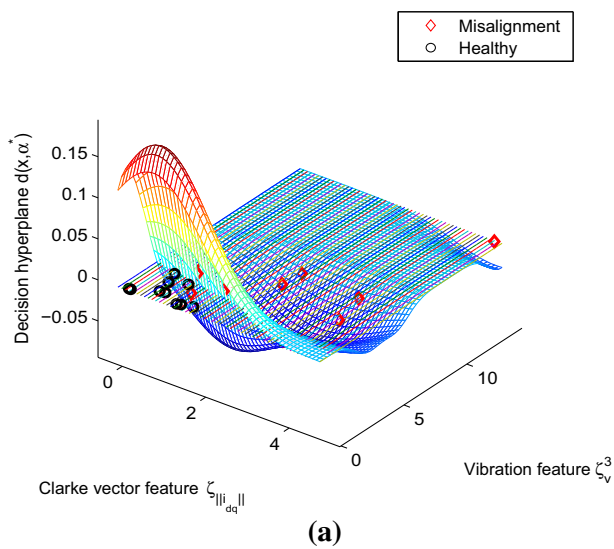


Fig. 9 **a** Decision surface $d(\mathbf{x}, \alpha^*)$ for binary classification of case: healthy vs. misalignment, **b** separation of healthy and misalignment data sets

6.3 Experimental validation

The results of the diagnostic scheme for the validation stage are shown in Tables 2 and 3, where the best accuracies are highlighted. These tables present the percentages of correct classification as a function of the parameter σ in the RBF in (6). The algorithm is tested considering the 4 IM conditions: healthy, unbalance, misalignment and bearing fault. As a result, a total of $25 \times 4 = 100$ operating regimes were evaluated, which were not used for training in the bootstrapped technique. Hence, Tables 2 and 3 show a good classification performance in the range of 84.8 to 100% under the variable operating condition regime. The worst classification ratio is obtained by the classifier of healthy and misalignment. While

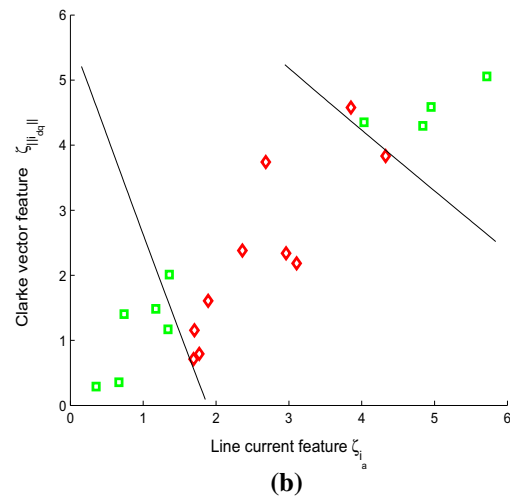
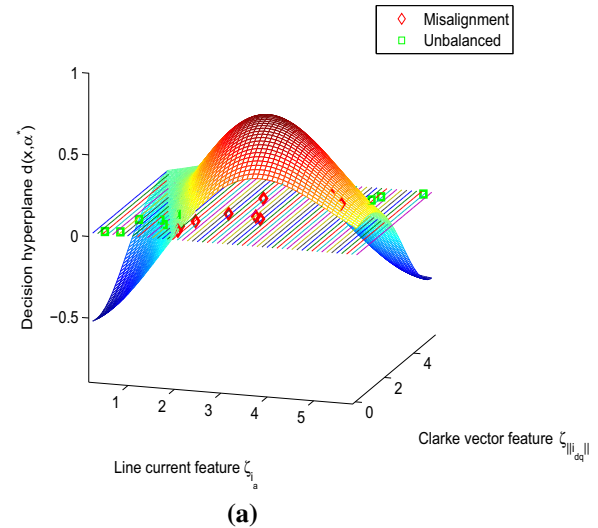


Fig. 10 **a** Decision surface $d(\mathbf{x}, \alpha^*)$ for binary classification of case: unbalance vs. misalignment, **b** separation of unbalance rotor and misalignment data sets

the best classification ratio is obtained by the classifier of bearing and unbalanced faults.

The results indicate that the radial vibration signal together with the electrical diagnostic media, stator current and Clarke vector modulus is a good indicator of a fault condition in the IM. Consequently, the FDI strategy based on SVM classification with one-against-one procedure and bootstrapped samples to select the parameters σ 's in the RBF showed a good degree of generalization by the validation results in Tables 2 and 3.

By comparing with previous results, in [37], the authors obtained a classification accuracy of 97.98% in an SVM multi-classification scheme to detect four kinds of gear-box faults (two related to bearing degradation) by means of vibration signals. Similar accuracies are obtained in the

Table 2 Classification results with the proposed scheme for SVM1, SVM2 and SVM3

| σ | SVM1 healthy vs. misalignment | SVM2 healthy vs. unbalance | SVM3 healthy vs. bearing damage |
|----------|-------------------------------|----------------------------|---------------------------------|
| 2 | 84.8 | 93.2 | 98.8 |
| 3 | 81 | 93.4 | 97.6 |
| 4 | 72.6 | 93.2 | 95.8 |
| 5 | 66.6 | 93 | 94.2 |
| 6 | 68.4 | 93 | 93.2 |
| 7 | 61.4 | 92.6 | 93 |
| 8 | 59.6 | 91.8 | 92.2 |
| 9 | 56.8 | 90.8 | 89.2 |
| 10 | 58 | 89.8 | 86.6 |
| 11 | 58 | 88.4 | 84.8 |
| 12 | 56 | 86.4 | 82.6 |
| 13 | 55.2 | 82.4 | 81.8 |

Table 3 Classification results with the proposed scheme for SVM4, SVM5 and SVM6

| σ | SVM4 misalignment vs. unbalance | SVM5 misalignment vs. bearing damage | SVM6 bearing damage vs. unbalance |
|----------|---------------------------------|--------------------------------------|-----------------------------------|
| 2 | 97.8 | 99.4 | 100 |
| 3 | 96.8 | 99.4 | 100 |
| 4 | 94.4 | 97.4 | 97.6 |
| 5 | 93.8 | 95.8 | 95.2 |
| 6 | 92.6 | 96 | 93 |
| 7 | 92.8 | 95.6 | 93.4 |
| 8 | 92.8 | 95.8 | 93 |
| 9 | 93.2 | 96.2 | 93 |
| 10 | 93.2 | 96 | 91.6 |
| 11 | 93.4 | 97.2 | 89.8 |
| 12 | 92.8 | 95.8 | 90.6 |
| 13 | 92.4 | 96.4 | 86.6 |

present study with 98.8, 99.4 and 100% for SVMs classifying bearing faults. These good classification accuracies are attributed to the structure of the features vector \mathbf{x} in (21) that incorporates mechanical and electrical fault signatures. However, this scheme presented some difficulty in distinguishing a misalignment fault from a healthy condition, which produced an accuracy of 84.8%. In [44], a multi-fault classification scheme is presented using current signatures to diagnostic broken rotor bars, supply voltage asymmetry, air-gap eccentricity and outer raceway ball bearing defects, with a classification accuracy rate of 95%. Hence, similar accuracies are obtained in the presented work for multi-fault classification, although the studied faults were not similar.

7 Conclusions

In this paper, we proposed a fault diagnosis algorithm based on SVMs for multi-fault classification of four IM

conditions (healthy, bearing damage, unbalanced rotor and misalignment). These conditions have been detected and isolated using a one-against-one multi-classification scheme. Our diagnosis scheme could detect the studied faults under variable operational conditions (supply frequency and load torque). The fault features extracted from electrical and mechanical diagnostic media were used as inputs for the SVMs, which perform the features data fusion. This data fusion capability improved largely the reliability of the proposed scheme compared to previous efforts in the field. The optimal parameters of the SVMs were obtained using a bootstrapped technique to minimize the error classification for different training datasets. We trained and tested our diagnosis algorithm with 10 and 25 different operating conditions, respectively, of the induction motor for the studied scenarios (140 conditions including a no-fault scenario) to validate our conclusions. Hence, the proposed diagnosis features (frequency components of stator current, radial vibration and Clarke vector modulus) allowed multiple-fault detection at

different operating conditions of the IM. In fact, just using radial vibration or MCSA, the diagnosis task could not be achieved effectively, so our contribution relied on combining electrical and mechanical diagnostic features to accomplish our goal. The FDI scheme was implemented in LabView for a real-time diagnosis, which highlights the applicability of the proposed FDI scheme for an industrial setting.

On the other hand, since the frequency information of the diagnosis features did not depend on the power rating of the IM, this FDI approach could be scaled to larger machines. Nonetheless, for larger IMs, the magnitudes of the supply voltages and currents will be increased, and most likely the baseline radial vibration signal. As a result, to re-scale the diagnosis approach, only the healthy information of the IM is required to normalize all the fault indexes. This observation will be the focus of future research. Meanwhile, the main drawback of the suggested FDI strategy is the limitation to extend the algorithm to study more faults, since the number of SVMs will have to increase, and most likely, also the number of features for classification; in addition, a new training procedure is required. Nevertheless, as future work, to extend the proposed FDI scheme, we will pursue to study short circuit faults in stator windings and eccentricity, and also to address the diagnosis problem in transient state and fault identification.

References

- Campos-Delgado DU, Espinoza-Trejo DR, Palacios E (2008) Fault tolerant control in variable speed drives: a survey. *IET Electr Power Appl* 2:121–134
- Nandi S, Toliyat HA, Li X (2005) Condition monitoring and fault diagnosis of electrical motors—a review. *IEEE Trans Energy Convers* 20:719–729
- Scheffer C, Girdhar P (2004) Practical machinery vibration, analysis & predictive maintenance. Newnes, Burlington, pp 89–115
- Cruz SM, Marques Cardoso AJ (2000) Rotor cage fault diagnosis in three-phase induction motors by extended park's vector approach. *Electr Power Compon Syst* 28:289–299
- Campos-Delgado DU, Murguía JS, Ramírez-Rodríguez O, Palacios E (2011) Quantitative and redundant multivariable fault diagnosis in induction motors. *Electr Power Compon Syst* 39:491–509
- Eltabacha M, Charara A (2007) Comparative investigation of electric signal analyses methods for mechanical fault detection in induction motors. *Electr Power Compon Syst* 35:1161–1180
- Eltabach M, Charara A, Zein I (2004) A comparison of external and internal methods of signal spectral analysis for broken rotor bars detection in induction motors. *IEEE Trans Ind Electron* 51:107–121
- Yilmaz I, Ayiek E, Senol I (2009) An experimental study about detection of bearing defects in inverter fed small induction motors by Concordia transform. *J Intell Manuf* 20:243–247
- Faiz J, Ebrahimi BM, Akin B, Toliyat HA (2010) Dynamic analysis of mixed eccentricity signatures at various operating points and scrutiny of related indices for induction motors. *IET Electr Power Appl* 4:1–16
- Cusido J, Romeral L, Ortega JA, Garcia A, Riba JR (2010) Wavelet and PDD as fault detection techniques. *Electr Power Syst Res* 80:915–924
- Unsal A, Kabul A (2016) Detection of the broken rotor bars of squirrel-cage induction motors based on normalized least mean square filter and Hilbert envelope analysis. *Electr Eng* 98(3):245–256
- Su H, Chong K, Parlos AG (2005) A neural network method for induction machine fault detection with vibration signal. *Lect Notes Comput Sci* 3481:1293–1302
- Riley CM, Lin BK, Habetler TG, Kliman GB (1999) Stator current harmonics and their causal vibrations: a preliminary investigation of sensorless vibration monitoring applications. *IEEE Trans Ind Appl* 35:94–99
- Schoen RS, Habelter TG, Kamran F, Bartheld RG (1995) Motor bearing damage detection using stator current monitoring. *IEEE Trans Ind Appl* 31:1274–1279
- Concari C, Franceschini G, Tassoni C (2008) Differential diagnosis based on multivariable monitoring to assess induction motor machine rotor conditions. *IEEE Trans Ind Electron* 55:4156–4166
- Kar C, Mohanty AR (2008) Vibration and current transient monitoring for gearbox fault detection using multiresolution Fourier transform. *J Sound Vib* 311:109–113
- Yang Z, Merrild U, Runge MT, Pedersen G, Borsting H (2009) A study of rolling-element bearing fault diagnosis using motor's vibration and current signatures. In: Proceedings of 7th IFAC symposium on fault detection, supervision and safety of technical processes, SAFEPROCESS'09, Barcelona, Spain, pp 354–359
- Contreras-Medina LM, Romero-Troncoso RJ, Cabal-Yepez E, Rangel-Magdaleno JJ, Millan-Almaraz JR (2010) FPGA-based multiple-channel vibration analyzer for industrial applications in induction motor failure detection. *IEEE Trans Instrum Meas* 59:63–72
- Sahoo S, Rodriguez P, Sulowicz M (2016) Evaluation of different monitoring parameters for synchronous machine fault diagnostics. *Electr Eng* 1–10. doi:10.1007/s00202-016-0381-6
- Hocine L, Nora Z, Samira K-M (2015) Wind turbine gearbox fault diagnosis based on symmetrical components and frequency domain. *Electr Eng* 97(4):327–336
- Urresty J-C, Riba J-R, Romeral L, Ortega JA (2015) Mixed resistive unbalance and winding inter-turn faults model of permanent magnet synchronous motors. *Electr Eng* 97(1):75–85
- Gao XZ, Ovaska SJ (2001) Soft computing methods in motor fault diagnosis. *Appl Soft Comput* 1:73–81
- Guo Q, Li X, Yu H, Hu W, Hu J (2008) Broken rotor bars fault detection in induction motors using Park's vector modulus and FWNN approach. *Lect Notes Comput Sci* 5264:809–821
- Zio E, Baraldi P, Gola G (2008) Feature-based classifier ensembles for diagnosing multiple faults in rotating machinery. *Appl Soft Comput* 8:1365–1380
- Ghate VN, Dudul SV (2010) Optimal MLP neural network classifier for fault detection of three phase induction motor. *Expert Syst Appl* 37:3468–3481
- Sakthivel NR, Sugumaran V, Babudevasenapati S (2010) Vibration based fault diagnosis of monoblock centrifugal pump using decision tree. *Expert Syst Appl* 37:4040–4049
- Kankar PK, Sharma SC, Harsha SP (2011) Fault diagnosis of ball bearings using machine learning techniques. *Expert Syst Appl* 38:1876–1886
- Lin J, Liu J, Li C, Tsai L, Chung H (2010) Motor shaft misalignment detection using multiscale entropy with wavelet denoising. *Expert Syst Appl* 37:7200–7204
- Martinez-Morales JD, Palacios E, Campos Delgado DU (2010) Data fusion for multiple mechanical fault diagnosis in induction motors at variable operating conditions. In: 7th International con-

- ference on electrical engineering, computing science and automatic control (CCE 2010), Mexico, pp 176–181
30. Konar P, Chattopadhyay P (2011) Bearing fault detection of induction motor using wavelet and Support Vector Machines (SVMs). *Appl Soft Comput* 11:4203–4211
 31. Rabelo-Baccarini LM, Rocha-e-Silva VV, Rodrigues-de-Menezes B, Matos-Caminhas W (2011) SVM practical industrial application for mechanical faults. *Expert Syst Appl* 38:6980–6984
 32. Kurek J, Osowski S (2009) Support vector machine for fault diagnosis of the broken rotor bars of squirrel-cage induction motor. *J Neural Comput Appl* 19:557–564
 33. Guo X, Long Z, He L, Hui Z, Wei G (2010) A comparative study on ApEn, SampEn and their fuzzy counterparts in a multiscale framework for feature extraction. *J Zhejiang Univ SCI A: Appl Phys Eng* 14:270–279
 34. Nguyen NT, Lee HH (2008) An application of support vector machines for induction motor fault diagnosis with using genetic algorithm. *Lect Notes Comput Sci* 5227:190–200
 35. Zhang XL, Chen XF, He ZJ (2010) Fault diagnosis based on support vector machines with parameter optimization by an ant colony algorithm. *Proc Inst Mech Eng Part C: J Mech Eng Sci* 224:217–229
 36. Wandekokem ED, Varejao FM, Rauber TW (2010) An overproduce-and-choose strategy to create classifier ensembles with tuned SVM parameters applied to real-world fault diagnosis. *Lect Notes Comput Sci Prog Pattern Recognit Image Anal Comput Vis Appl* 6419:500–508
 37. Fafa C, Baoping T, Renxiang C (2013) A novel fault diagnosis model for gearbox based on wavelet support vector machine with immune genetic algorithm. *Measurement* 46(1):220–232
 38. Zhiwen L, Hongrui C, Xuefeng C, Zhengjia H, Zhongjie S (2013) Multi-fault classification based on wavelet SVM with PSO algorithm to analyze vibration signals from rolling element bearings. *Neurocomputing* 99:399–410
 39. Samanta B, Nataraj C (2009) Use of particle swarm optimization for machinery fault detection. *Eng Appl Artif Intell* 22(2):308–316
 40. Hwang D-H, Youn Y-W, Sun J-H, Choi K-H, Lee J-H, Kim Y-H (2015) Support Vector Machine based bearing fault diagnosis for induction motors using vibration signals. *J Electr Eng Technol* 1:30–40
 41. Seshadrinath J, Singh B, Panigrahi BK (2014) Investigation of vibration signatures for multiple fault diagnosis in variable frequency drives using complex wavelets. *IEEE Trans Power Electron* 29(2):936–945
 42. Vapnik V (1998) *Statistical learning theory*. Wiley, New York, pp 219–232
 43. Efron B, Tibshirani R (1993) *An introduction to the bootstrap*. Chapman & Hall, New York
 44. Bacha K, Salem S, Chaari A (2012) An improved combination of Hilbert and Park transforms for fault detection and identification in three-phase induction motors. *Electr Power Energy Syst* 43:10061016
 45. Xu L, Anan Z, Xunan Z, Chenchen L, Li Z (2013) Rolling element bearing fault detection using support vector machine with improved ant colony optimization. *Measurement* 46(8):2726–2734